Minerals Engineering 123 (2018) 35–48

Contents lists available at ScienceDirect

Minerals Engineering

journal homepage: www.elsevier.com/locate/mineng

Modes of occurrences of scandium in Greek bauxite and bauxite residue

Johannes Vind[a,b,*], Annelies Malfliet[c], Chiara Bonomi[b], Päärn Paiste[d], István E. Sajó[e], Bart Blanpain[c], Alan H. Tkaczyk[f], Vicky Vassiliadou[a], Dimitrios Panias[b]

[a] Department of Continuous Improvement and Systems Management, Aluminium of Greece Plant, Metallurgy Business Unit, Mytilineos S.A., Agios Nikolaos, 32003 Viotia, Greece
[b] School of Mining and Metallurgical Engineering, National Technical University of Athens, Iroon Polytechniou 9, 15780, Zografou Campus, Athens, Greece
[c] Department of Materials Engineering, KU Leuven, Kasteelpark Arenberg 44, P.O. Box 2450, B-3001 Leuven, Belgium
[d] Department of Geology, University of Tartu, Ravila 14A, 50411 Tartu, Estonia
[e] University of Pécs, Szentágothai Research Centre, Pécs, H-7624, Ifjúság str. 20, Hungary
[f] Institute of Physics, University of Tartu, Ostwaldi 1, 50411 Tartu, Estonia

ARTICLE INFO

Keywords:
Karst bauxite
Bauxite residue
Red mud
Scandium
Hematite
Goethite
Zircon
Bayer process

ABSTRACT

Bauxite and bauxite residue, a by-product of alumina production, were studied using a combination of micro-analytical techniques — electron microprobe wavelength dispersive spectrometry, laser ablation inductively coupled plasma mass spectrometry and μ-Raman spectroscopy. The aim of the work was to reveal the modes of occurrence of scandium (Sc). The motivation behind this effort was to provide mineralogical insight for the support of ongoing development of Sc extraction technologies from bauxite residue. In the analyzed bauxites and residue, Sc is mainly hosted in hematite, where Sc^{3+} probably substitutes Fe^{3+}. The average concentration of Sc in the hematite matrix of bauxite is about 200 mg/kg, while in the bulk sample it ranges from 42 to 53 mg/kg Sc. In bauxite residue, the average concentration of Sc in hematite matrix is about 170 mg/kg, and in the bulk sample it is 98 mg/kg. In bauxite residue, goethite was also identified to host Sc with a concentration of about two times more than in hematite — 330 mg/kg. In bauxite residue, hematite, goethite and zircon host respectively 55 ± 20%, 25 ± 20% and 10 ± 5% of the total Sc. The effect of the Bayer process to the modes of occurrences of Sc is minor. The secondary bauxite residue minerals formed during bauxite processing do not capture any or capture very low amounts of Sc. New evidences of Sc leaching behavior from bauxite residue show that Sc is first released from goethite, then from hematite and the unrecovered proportion of Sc is likely associated with zircon.

1. Introduction

Scandium (Sc) has found its way to several advanced applications such as solid oxide fuel cells and Sc-Al alloys because of its unique properties. Despite its use in several applications, the production of Sc remains low, about 10–15 tons per year. It is mainly extracted as a by-product from uranium (U), titanium (Ti), rare earth elements (REE) and apatite production (Gambogi, 2017; Samson and Chassé, 2016). European Commission considers Sc as one of the 26 critical raw materials (European Commission et al., 2017). This means that it has high economic importance while also having high supply risk.

The presence and relative abundance of Sc in bauxites as well as in bauxite residue, a by-product of alumina production, have been acknowledged for decades (Ochsenkühn-Petropulu et al., 1994; Wagh and Pinnock, 1987). However, no large-scale production from these resources has taken place (Gambogi, 2017). There is a variety of technologies available for the extraction of Sc from bauxite residue and they have been summarized elsewhere (Akcil et al., 2017; Binnemans et al., 2015; Borra et al., 2016; Davris et al., 2017; Liu and Li, 2015; Zhang et al., 2016). It has been estimated that 70% of the world's Sc resources might be found in bauxites (Lavrenchuk et al., 2004). Given that the Bayer process enriches the contents of Sc from bauxite to its residues by a factor of about two, it could be an attractive secondary resource of Sc (Ochsenkühn-Petropulu et al., 1994; Vind et al., 2018). Moreover, an increasing volume of research is attempting to find feasible methods for turning bauxite residue into value-added products, rather than dumping this by-product into disposal areas (Binnemans et al., 2015; Borra et al., 2016; Davris et al., 2017; Evans, 2016). Despite the interest in Sc extraction, very few studies have been conducted to empirically uncover the modes of occurrences of Sc in bauxite residue and studies

* Corresponding author at: Department of Continuous Improvement and Systems Management, Aluminium of Greece Plant, Metallurgy Business Unit, Mytilineos S.A., Agios Nikolaos, 32003 Viotia, Greece.
E-mail address: johannes.vind@alhellas.gr (J. Vind).

https://doi.org/10.1016/j.mineng.2018.04.025
Received 15 December 2017; Received in revised form 21 April 2018; Accepted 23 April 2018
Available online 30 April 2018

that have targeted this question in bauxite itself are even scarcer (Suss et al., 2017; Zhang et al., 2017, 2016).

The objective of this work is to reveal the modes of occurrences of Sc mainly in bauxite residue as well as in bauxites that represent the parent materials from which the residue is derived from. The primary focus of this paper is therefore on the characterization of Sc in bauxite residue from Aluminium of Greece as well as in Sc-enriched bauxites that they exploit. Explaining the forms in which Sc occurs in bauxite residue minerals will aid the design of Sc extraction technologies from these resources as well as explain, why high recovery rates during Sc extraction are difficult to achieve. A brief literature review is given to provide the state of the art knowledge existing in the field.

2. Geological and geochemical background

Within the geochemical cycle, Sc is known to be present in mafic and ultramafic rocks rather than in felsic rocks. Sedimentary rocks commonly exhibit a very low content of Sc. However, some bauxites and laterites are relatively rich in Sc. Its average concentration in continental crust is 22 mg/kg (Rudnick and Gao, 2003). Sc behaves as a lithophile element and is not affected by the redox conditions of the environment. Sc does not exhibit affinity towards ore forming anions. Because of that, it can be found in small quantities dispersed in many rock forming minerals rather than concentrated in independent mineral phases. Such phases exist (e.g. kolbeckite, thortveitite), but are very rare. Since Sc is scattered in the Earth's crust and deposits with high Sc grade are not formed in natural processes, the production of Sc has relied on resources with Sc content around 100 mg/kg Sc (Das et al., 1971; Samson and Chassé, 2016).

When Sc is present in a bauxite deposit, its distribution is typically associated with REEs, as in south Italian and Sardinian karst bauxite deposits. This distribution pattern is interpreted as a covariance due to the chemical similarities of REEs and Sc rather than as an indication of the formation of any specific Sc-bearing mineral (Blankova et al., 1977; Mongelli et al., 2017). In the Zagrad bauxite deposit (Montenegro), Sc was enriched throughout the bauxite profiles, while some of the lower parts of profiles were particularly enriched in Sc as well as in REEs content (Radusinović et al., 2017).

2.1. Parnassos-Ghiona bauxite deposit

Parnassos-Ghiona bauxite deposit is located in Central Greece, north of the Gulf of Corinth. The bauxite deposit consists of three consecutive horizons as layers, pockets or irregular bodies intercalated in Mesozoic limestones. Because the genesis of the deposit is related to limestones and karst phenomena, it is categorized as a karst bauxite deposit (Bárdossy, 1982; Petrascheck, 1989; Laskou and Economou-Eliopoulos, 2007; Mettos et al., 2008; Valeton et al., 1987). A recent review and a case study of the deposit, with an emphasis on REEs occurrence, is compiled by Deady et al. (2016). The overall average Sc concentration in Greek bauxites is 46 ± 18 mg/kg (sample population n = 30) (Laskou and Economou-Eliopoulos, 2007; Laskou, 1991; Ochsenkühn-Petropulu et al., 1994; Laskou and Economou-Eliopoulos, 2013).

3. Bayer process and bauxite residue

The Bayer process is the primary method by which alumina (Al_2O_3) is produced from bauxite ore. In this hydrometallurgical process, caustic soda digestion under elevated temperature and pressure is used to leach soluble alumina minerals from the bauxite ore and subsequently precipitate technically pure aluminum hydroxide. From the pregnant leach solution, the residual mineral matrix is removed as a by-product, commonly termed as bauxite residue or "red mud" (Adamson et al., 2013; Gräfe and Klauber, 2011). The global annual production of bauxite residue is estimated to be about 150 Mt (Evans, 2016). In the process flowsheet of Aluminium of Greece, Metallurgy Business Unit, Mytilineos S.A., (AoG), about 80% of the bauxite feed is from karst bauxite, mainly Greek origin. About 20% of feed is from lateritic bauxite originating from West Africa (Ghana, Awaso) or Brazil (Porto Trombetas). The method where the hard-to-leach karst (diasporic/boehmitic) bauxite and easily leachable lateritic (gibbsitic) bauxite are used simultaneously in an alumina plant is known as the "sweetening" process. The suspended karst bauxite is digested at a high temperature, and then the lateritic bauxite suspension stream is introduced to the main karst bauxite slurry stream in the appropriate flashing stage. "Sweetening" is utilized to increase the productivity of the plant (Lavalou et al., 1999). The karst bauxite slurry in AoG is digested at about 255 °C (Balomenos et al., 2009) and a pressure of about 5.8–6.0 MPa.

Sc concentrations detected in bauxite residues worldwide range from 41 to 254 mg/kg (Borra et al., 2016; Zhang et al., 2016). Based on various publications that used different analytical techniques, the average concentration of Sc in AoG's bauxite residue is 121 ± 16 mg/kg (n = 24) (Alkan et al., 2017; Borra et al., 2015; Davris et al., 2014, 2016; Gamaletsos et al., 2016b; Laskou and Economou-Eliopoulos, 2013; Lymperopoulou et al., 2017; Ochsenkühn-Petropulu et al., 1994; Vind et al., 2017; Yagmurlu et al., 2017). It has been reported that over a 15-year period, the concentration of rare earth elements (REE) as well as Sc in the bauxite residue of AoG has fluctuated only about 8%, indicating to a stable and homogeneous occurrence of Sc in this material (Davris et al., 2017). By 2015, the volume of bauxite residue accumulated in Greece was estimated to be about 5 Mt, resulting from the yearly output of 0.7 Mt (Anagnostou, 2010; Deady et al., 2016). Based on the preceding information, the amount of Sc present in AoG's bauxite residue stocks could be about 600 tons in total.

4. Reports on the modes of occurrences of Sc in bauxite-bauxite residue system

4.1. By indirect methods

Several mineral hosts of Sc have been suggested for bauxite and its residue system. A correlation between Sc and P_2O_5 occurrence has been reported at least in three cases. Phosphate phases, like variscite, have been considered as Sc host minerals (Radusinović et al., 2017; Suss et al., 2017; Wagh and Pinnock, 1987).

Derevyankin et al. deduced from their analysis of Sc behavior in the Bayer process that Sc is most likely bound with iron oxides and titanium dioxides in bauxite (Derevyankin et al., 1981). Correlations between Ti and Sc behavior during leaching tests and the assumed mineralogical association of these metals have been reported at least three times for the case of AoG's bauxite residue (Bonomi et al., 2017b; Ochsenkühn-Petropulu et al., 1994; Rivera et al., 2017).

Mongelli et al. suggested on the basis of established association of Sc^{3+} with Fe^{3+} and geochemical data of several Italian bauxite deposits that Sc might occur in detrital iron minerals like titanomagnetite (Mongelli et al., 2017). It was hypothesized that Sc might be bound to iron oxides of bauxite residue, either by substituting Fe^{3+} or by its adsorption on iron oxides mineral surfaces, by analyzing the behavior of Sc during leaching experiments (Borra et al., 2015).

4.2. By direct methods

As the result of direct investigation by electron microprobe, the first reports referring to Sc occurrence in certain bauxite minerals date back to 1973 and indicate its presence in detrital zircon (Bárdossy and Pantó, 1973). It is a well-established fact that Sc can be found in zircon, as reported in several bauxite deposits: Mazaugues (France), Campo Felice (Italy), bauxites of Southern Apennines (Italy) (Bárdossy and Pantó, 1973; Boni et al., 2013; Mongelli et al., 2017; Radusinović et al., 2017). In Schugorsk deposit (Urals, Russia), zircon grains exhibited altered rims that contained up to 3.5 wt% Sc (Mordberg et al., 2001). The

multivalent substitution in zircon is commonly explained as $Zr^{4+} + Si^{4+} \leftrightarrow Sc^{3+} + P^{5+}$. Calcium (Ca) as well as yttrium (Y) are also sometimes substituted in zircon (Breiter et al., 2006).

Authigenic xenotime (YPO_4) of Zagrad bauxite deposit (Montenegro) has been shown to contain some amount of Sc (0.4–0.6 wt%) while residual xenotime did not contain any (Radusinović et al., 2017).

In Middle Timan bauxite (Urals, Russia), up to 55–60% of Sc is associated with diaspore and boehmite, where its concentration ranges from 100 to 110 mg/kg. The remaining part is found in zircon and chamosite, while the concentrations of Sc in these minerals are not known. During Bayer digestion, Sc is released from diaspore and boehmite and is thereafter assumed to be adsorbed on the surface of bauxite residue particles as ScO(OH) or $Sc(OH)_3$ (Suss et al., 2017).

Xiao has concluded after combining the results of leaching experiments and electron microprobe analyses of BR from Guizhou Alumina Production (China) that Sc in bauxite residue is associated with anatase, rutile, ilmenite, zircon and monazite by isomorphic substitution while other forms were excluded ((Xiao, 1996) cited in (Zhang et al., 2017)). On the other hand, Zhang et al. (2017) concluded on the basis of bauxite residue from Shandong Alumina Refining Plant (China), that Sc is exclusively associated with iron phases represented by hematite and goethite in the residue. In that assessment, no distinction is made between the two iron phases (Zhang et al., 2017). Some deficiencies in the explanations of the experimental setup can hinder the reproducibility of their work.

5. Materials and methods

The present assessment is based on the bauxites exploited and bauxite residue produced by AoG. All types of bauxites utilized by AoG were screened for the content of Sc to identify the main inputs of Sc to the process. That included diasporic bauxites mined in Greece and two samples of lateritic bauxites, one from Brazil (Porto Trombetas) and the other from Ghana (Awaso deposit). Bauxite residue as the main output carrier of Sc from the Bayer process (Vind et al., 2018) was analyzed as the primary material of interest. Bauxite samples were separated from one-ton test batches of bauxite feed, that is the method by which a refinery characterizes its raw material to ensure the quality of the ore. Bauxite residue was collected in the form of a filtered cake after the dewatering of the washed bauxite residue in the filter presses which is the current practice in AoG's plant. It was collected as a composite sample of appropriate number of sub-samples. Concerning the representativeness of the bauxite residue sample, we rely on the long-term and ongoing experience on REEs as well as Sc research relating to AoG's bauxite residue. It has been reported that the variation in the concentrations of the REEs as well as Sc in AoG's bauxite residue has been only about 8% during a 15-year period (Davris et al., 2017). This provides an insight that the residue from AoG is a relatively homogeneous material, concerning the occurrence of critical metals such as Sc. All materials, bauxite and its residues, were dried, split and homogenized using standard sampling techniques. Bauxite samples (ST and DD) originating from Greek Parnassos-Ghiona deposit B3 horizon represent the principal material feed used by AoG. Bauxite DD and bauxite ST are from different Greek mines and samples were collected from AoG's stockpiles. Bauxite ST is extracted from the deposit by S&B Industrial Minerals S.A., and bauxite DD by Delphi-Distomon S.A., a subsidiary of Mytilineos S.A. An additional scale sample from the autoclaves of the Bayer process was collected for complementary analyses. Scales formed in the piping and autoclaves of the Bayer refineries are considered as minor by-products that can reveal characteristics of the Bayer process specific mineral phases, which are also commonly the main components of scales (Bánvölgyi, 2016; Kawashima et al., 2016; Zhong-Lin and Song-Qing, 1995). In relation to trace elements, perovskite-based scale has been reported to contain small amounts of Y, Nb and Zr, for example (Zhong-Lin and Song-Qing, 1995).

Based on their elevated Sc content, four principal samples were subjected to a detailed microscale investigation: (1) Greek Parnassos-Ghiona bauxite ST, (2) Greek Parnassos-Ghiona bauxite DD, (3) bauxite residue, and (4) scale formed in the digester autoclave. The samples subjected to microscale analyses were embedded in resin, cut and polished to create cross sections and then coated with platinum. They were prepared as well as analyzed in duplicate.

The bulk chemical composition of the main elements was determined by standardized X-ray fluorescence (XRF), Cr and V were analyzed by inductively coupled plasma mass spectrometry (ICP-MS) after lithium metaborate/tetraborate fusion. Sc was analyzed in Activation Laboratories Ltd. (Ancaster, ON, Canada) by instrumental neutron activation analysis (INAA). The latter method was preferred over ICP-MS because of the previously reported discrepancies in Sc behavior during ICP-MS analysis in bauxite and bauxite residue matrices (Feret and See, 2010). Mineralogical composition was identified by X-ray diffraction (XRD) with a Brucker D8 Focus instrument. Phase composition was identified and quantified using the XDB Powder Diffraction Phase Analytical System (Sajó, 2008, 2005). The estimated relative error for phase quantification is 10% (Sajó, 2008).

Preliminary microscale analyses were performed with scanning electron microscopy with energy dispersive spectroscopy (SEM-EDS; EVO MA15 coupled with AZtec X-MAX 80). Electron probe microanalysis coupled with wavelength dispersive spectroscopy (EPMA-WDS) was applied by using JEOL JXA-8530F instrument. Four analyzing crystals were used: (1) TAP, (2) TAPH, (3) PETH, and (4) LIFH. The accelerating voltage was 15 kV and the beam current either 100 nA for typical observations or 50 nA (a few cases 15 nA) for areas exhibiting sensitivity to a high current. For a regular WDS quantification, counting time on peak was 60 s and on background 10 s. Long counting times (60 s), high beam current (100 nA) and usage of the H-type spectrometers resulted in an estimated detection limit of Sc of about 10 mg/kg. EPMA-WDS quantifications were carried out using the standards listed in Table 1.

Complementary in-situ Sc content quantification was performed by laser ablation (LA) ICP-MS (Cetac LSX-213 G2 + LA, HelEx 2- vol ablation cell, coupled to Agilent 8800 ICP-MS). Helium was used as carrier gas at combined flow of 0.8 L/min. USGS GSD-1G standard was used for quantification and BHVO-2G and NIST612 were used for quality control measurements. Iron (Fe) was used as an internal standard element for the analysis of hematite matrices and aluminum (Al) in the case of aluminum oxyhydroxide matrices. Internal standard element concentrations were determined by SEM-EDS quantitative measurements as average values of the representative sample areas. Single spot analyses with spot size of 40 µm, laser energy output of 1.46–1.48 J/cm^2 at a frequency of 10 Hz were used.

In-situ phase identification was performed by µ-Raman spectroscopy, using a Renishaw inVia confocal Raman microscope, operated with a 785-nm laser at a power of 25–50 mW at laser source. Positions

Table 1
Standards used in EPMA-WDS quantification.

Element	Standard	Formula
Sc	Scandium metal	Sc
Fe	Hematite	Fe_2O_3
Ti	Rutile	TiO_2
Zr	Zirconia cubic	ZrO_2
Al	Albite	$Na(AlSi_3O_8)$
Na	Albite	
Ca	Diopside	$CaMgSi_2O_6$
Mg	Periclase	MgO
Mn	Willemite	$(Zn,Mn)_2SiO_4$
Cr	Chromium (III) oxide	Cr_2O_3
V	Vanadium (III) oxide	V_2O_3
Hf	*Internal standard*	
U	*Internal standard*	

Table 2
Bulk chemical composition of the studied samples.

Sample	LOI %	Al_2O_3 %	Fe_2O_3 %	SiO_2 %	TiO_2 %	CaO %	Na_2O %	Cr mg/kg	V mg/kg	Sc mg/kg
Bauxite ST	11.29	58.34	21.01	2.48	2.66	1.73	n/a	588	537	42.4
Bauxite DD	12.62	59.90	20.43	3.02	2.87	0.46	n/a	693	336	52.8
Bauxite Awaso	25.0	52.73	13.54	4.29	1.49	< 0.01	n/a	521	221	8.6
Bauxite Porto Trombetas	28.0	53.73	11.19	4.96	1.35	< 0.01	n/a	138	201	7.0
Bauxite residue	9.17	20.64	41.65	6.76	5.32	10.07	2.87	1429	1029	97.6
Autoclave scale	8.0	25.77	7.55	25.60	4.39	3.67	22.43	398	225	19.7

of the areas of interest were located with a Leica microscope coupled to the Raman microscope. The Raman spectra were processed with Spectragryph 1.0.7 software (Menges, 2017). Reference data was retrieved from RRUFF database (Lafuente et al., 2015).

The experimental setup of the leaching experiment is described by Bonomi et al. (2017a) and by Bonomi et al. (2017b). Briefly, the direct leaching of bauxite residue was performed by using a hydrophilic ionic liquid [Emim][HSO_4] at a 5% pulp density under different temperatures and stirring rates.

5.1. Challenges in the microanalysis of bauxite residue

When performing microscale analysis of bauxite residue, some limiting conditions should be considered. First, the particle size of bauxite residue is very fine. In AoG's bauxite residue, 80% of the particles are below 1 μm in dimensions (Borra et al., 2015). The fineness of the residue material is partly caused by the crushing and milling of bauxite during the preprocessing of bauxite feed (e.g. Chin, 1988). The need for fine particle size is crucial during the exploitation of especially karst (diasporic/boehmitic) bauxites (Lavalou et al., 1999). The minimum particle size that can readily be studied in EPMA is about 1 μm. Therefore, about 20% of the particles can be analyzed with this technique. It is reported, however, that there is no significant partitioning of mineral phases between the different size fractions in AoG's bauxite residue. A slightly higher amount of gibbsite and diaspore may be present in the coarser fractions (125–325 μm) and a higher amount of hydrogarnet group phases in the finest fractions (< 32 μm). The results of phase composition were obtained by sieving the bauxite residue sample into four size fractions and then the relative XRD peak intensities of each of the fractions were compared (Pontikes, 2007). Besides, it has been reported from the beneficiation experiments of different bauxite residues that there is only a slight enrichment of Sc in the finest fraction (< 20 μm) of the material while the other fractions have relatively even distribution of Sc (Gu et al., 2016; Petrakova et al., 2014). To partly overcome the problem of fineness of bauxite residue, bauxite samples were studied which have not undergone crushing and grinding and therefore are not disturbed materials like the residue is. In order to analyze larger crystals of the specific Bayer process secondary minerals, a sample of scale from the digester autoclave was collected, which contained perovskite- and cancrinite-enriched matrices. Perovskite-based scales, for instance, have been previously shown to contain trace elements like Y, Nb and Zr (Zhong-Lin and Song-Qing, 1995). It has been also shown in other studies, that the investigation of Bayer process scales can provide advantageous information regarding the various properties of the secondary Bayer process mineral phases (Bánvölgyi, 2016; Kawashima et al., 2016). Besides that, bauxite residue was preliminarily investigated with transmission electron microscopy (TEM), which has the capability to make observations of nanoscaled materials. Unfortunately, the EDS device attached to TEM did not provide the required sensitivity to detect the low quantities of Sc in bauxite residue's fine particulates.

The second limiting condition for analyzing bauxite residue is that it can be a mixture of raw materials from different origins, as in the present case of AoG. Thus, it can be difficult to distinguish the origin of a particle. Also, for this reason were the significantly Sc-enriched source bauxites examined that provide the characteristics of the source material of bauxite residue. We consider our analysis to be representative for the bulk of AoG's bauxite residue, although further research can be suggested to characterize Sc in the < 1 μm fraction and advanced techniques such as the X-ray absorption near-edge structure (XANES) spectroscopy, synchrotron beamline μXRF and μXRD as well as nanoscale secondary ion mass spectrometry (nano-SIMS) methods could be considered.

6. Results and discussion

6.1. Bulk characterization

The analyzed bauxite samples are dark brown with a pisolithic texture. Sample ST is porous, DD is more massive than porous. Samples are chemically largely composed of aluminum and iron oxides (Table 2) and the main mineral phases are diaspore, boehmite and hematite (Table 3).

The main input of Sc to the Bayer process is from Greek diasporic bauxites (96%) (Vind et al., 2018), containing around 40–50 mg/kg Sc (Table 2). Lateritic bauxites originating from Brazil (Porto Trombetas) and Ghana (Awaso) were neglected in the detailed microscale study because of their low content of Sc (7 and 8.6 mg/kg, respectively). At the time of sampling, Brazilian bauxite was used as the lateritic bauxite feed with a proportion of 20% of the total feed.

Bauxite residue is a dark red thick muddy material with moisture content about 26% in its initial state. While bauxites are composed of well crystallized phases judging by the narrow peaks of XRD scans, the crystallinity of bauxite residue phases less developed as seen from the wider XRD peaks and therefore indicating to some XRD-amorphous content (Fig. 1). According to a previous work, about 10% of AoG's bauxite residue could be XRD amorphous (Hertel et al., 2016).

Chamosite was detected only in the bauxite residue sample, but its presence has been reported earlier in Parnassos-Ghiona bauxite (Laskou and Economou-Eliopoulos, 2007). The 2Θ positions of kaolinite and chamosite coincide on diffractograms of bauxites. Chamosite reacts very slowly in the Bayer process and does so at temperatures above 280 °C (Songqing and Zhonglin, 2016). Therefore, its presence in bauxite residue is expected.

Bauxite processing results in the formation of secondary minerals like hydrogarnet group phases. In the present sample we identified the phase being an iron substituted hydrogarnet ($Ca_3[Al,Fe]_2(SiO_4)_n{\cdot}(OH)_{12-4n}$) (Sajó, 2005; Smith, 2017). Nevertheless, it is reasonable to assume that several of the hydrogarnet group endmembers exist in bauxite residue since their XRD peak positions are similar. Perovskite phase ($CaTiO_3$) is the result of titanium dioxides, mainly anatase, reacting with NaOH and then with lime (Smith, 2017; Suss and Rydashevsky, 1996). The reaction between sodium aluminate and dissolved silica forms cancrinite ($Na_8(Al,Si)_{12}O_{24}(OH)_2{\cdot}3H_2O$) (Sajó, 2008; Whittington, 1996).

A rough indirect estimate of zircon phase quantity in the studied materials resulted in a value of 0.1% in bauxite and 0.2% in bauxite residue. This estimate was based on bulk zirconium (Zr) elemental

Table 3
Mineralogical composition of the studied bauxite and bauxite residue as well as autoclave scale samples, representing XRD-crystalline phases. Secondary phases formed during the Bayer process are in italics.

Sample	Boehmite %	Diaspore %	Hematite %	Goethite %	Anatase %	Rutile %	Calcite %	Quartz %	Kaolinite %	Chamosite %	Gibbsite %	*Hydrogarnet* %	*Cancrinite* %	*Perovskite* %	*Portlandite* %	Total %
Bauxite ST	32	36	17	4.5	2	0.7	3	0.5	3.5							99.2
Bauxite DD	53	14.5	17.5	3	2.2	0.7	0.8		6.5							98.2
Bauxite Ghana	1.5	1	3.5	9	0.4	1.2		0.3	2		80					98.9
Bauxite Trombetas			6	6	0.9	0.4			10.7		76					99.8
Bauxite residue	2	13	31	7.5	0.6	0.7	5	0.3		3.7	2.5	14.5	11	4	0.8	96.6
Autoclave scale[a]		1.5	6.5								0.7	4	74	7.5		100.2

[a] Also 2.5% sodalite and 3.5% $Na_2SO_4{\cdot}10H_2O$, both secondary products of the Bayer process.

concentration (0.12% Zr in bauxite residue) (Gamaletsos et al., 2016b), assuming that all of the elemental Zr is attributed to zircon mineral phase.

6.2. Scandium hosted in hematite and goethite

6.2.1. Bauxite

Iron phases are represented by hematite and goethite in both bauxite samples, as detected by XRD. It was determined qualitatively and quantitatively by EPMA-WDS that iron oxide matrices contain Sc in elevated concentrations when compared to the bulk Sc concentrations of the respective samples (Tables 2, 4, 5). The analyzed areas containing mainly iron oxide were chosen as those with the highest possible purity (e.g. Fig. 2 showing the area of LA-ICP-MS measurements). However, minor contribution from other compounds might have occurred because Al_2O_3, TiO_2 and SiO_2 impurities were also detected with both EPMA-WDS and LA-ICP-MS techniques. Al_2O_3 content might be from finely dispersed aluminum oxyhydroxide phases, SiO_2 because of kaolinite group phases contribution, and TiO_2 can be either because of the occurrence of Ti in hematite mineral lattice or due to the occurrence of nanoscale titanium dioxide phases in the matrix. The latter have been proven to exist in the diaspore matrix of Parnassos-Ghiona Fe-depleted bauxite (Gamaletsos et al., 2017).

A representative area of the iron oxide dominant matrix was identified to be hematite-dominant by μ-Raman spectroscopy (Fig. 3). It is possible to conclude that Raman bands at wavenumbers 225, 245, 292, 411, 496 and 610 cm^{-1} are attributed to hematite, when comparing the spectra with those presented literature and reference patterns measured with the same exciting laser wavelength (785 nm) reported by different authors (De Faria et al., 1997; Gamaletsos et al., 2007; Lafuente et al., 2015). Minor band at 450 cm^{-1} could represent diaspore (Gamaletsos et al., 2007; Ruan et al., 2001) and a band at 661 cm^{-1} could be attributed to magnetite. Because of its gaussian shape, the latter could also be a fluorescence peak. Magnetite has not been confirmed to appear in the bulk sample by XRD, but it might occur under the detection limit of this technique.

The average Sc concentration in the bauxite DD hematite-dominant matrices was higher (260 mg/kg) than that of the bauxite ST sample (170 mg/kg) (Table 4), measured by EPMA-WDS. Full data of the quantification are displayed in Tables A.1 and A.2. The standard deviation (S.D.) in Table 4 and in the following tables is calculated as the *sample standard deviation* for a better representation of the whole sample, considering the small number of performed measurements. The occasional high S.D. values in Table 4 and in following tables are due to the high spread of the measured values.

The presence of Sc in hematite matrices of bauxite was further confirmed by LA-ICP-MS measurements (Table 5). The two methods produced constant values for both samples. Sample DD with higher Sc contents in hematite areas yields also higher bulk concentration of Sc (Table 2). When comparing two methods, the average concentration of Sc in the hematite matrix of 200 mg/kg measured by EPMA-WDS was almost identical to the average value determined by LA-ICP-MS on both bauxite samples, 199 mg/kg (n = 9). The average Sc concentration contained in the hematite matrix equals to that of an Australian laterite deposit, where Sc content in hematite was also shown to be 200 mg/kg on average (Chassé et al., 2017). The most probable form of occurrence of Sc in hematite is by the known substitution of Fe^{3+} with Sc^{3+} (Chassé et al., 2017; Horovitz, 1975; Samson and Chassé, 2016). The occurrence of goethite was not revealed during microscale analysis of bauxite samples. Therefore, it was not possible to establish whether goethite hosts any Sc in bauxites or not. It could be that goethite occurs in these samples in sub-μm size. Laskou and Economou-Eliopoulos (2007) as well as Laskou and Economou-Eliopoulos (2013) have noted the presence of goethite in Parnassos-Ghiona bauxites in association with pyrite and diaspore in veins crosscutting the bauxite matrix as well as in small (~10 μm) cavities.

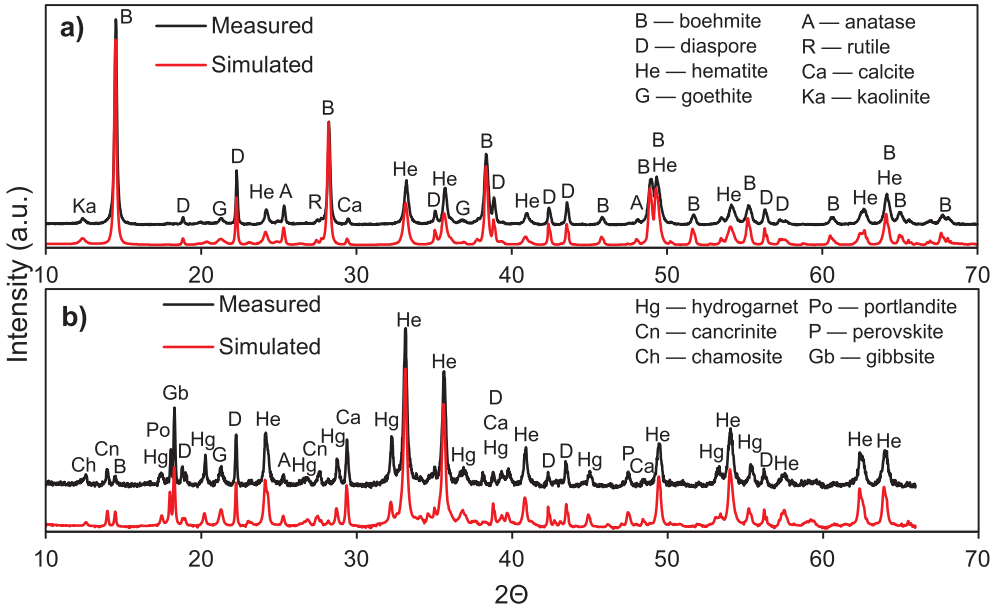

Fig. 1. Diffractograms and simulated patterns of (a) bauxite DD, and (b) bauxite residue.

Table 4
Chemical composition of hematite-dominant matrices of bauxite samples determined by EPMA-WDS. In the category "Greek bauxite overall", measurements of the two Greek Parnassos-Ghiona bauxite samples are combined.

Analyte	Bauxite DD (n = 12)			Bauxite ST (n = 16)			Greek bauxite overall (n = 28)		
	Median	Average	S.D.	Median	Average	S.D.	Median	Average	S.D.
Fe_2O_3 (wt%)	88.12	85.84	7.66	96.13	95.97	1.32	94.13	91.63	7.14
TiO_2 (wt%)	2.82	2.82	0.51	2.52	2.53	0.38	2.57	2.66	0.46
Al_2O_3 (wt%)	9.58	11.83	8.36	1.98	2.47	1.82	3.00	6.48	7.25
SiO_2 (wt%)	1.12	1.14	0.11	0.57	0.64	0.33	0.80	0.85	0.36
Na_2O (wt%)	0.00	0.01	0.01	0.02	0.02	0.01	0.01	0.01	0.01
CaO (wt%)	0.15	0.15	0.03	0.11	0.11	0.04	0.13	0.13	0.04
Cr_2O_3 (wt%)	0.22	0.22	0.04	0.18	0.20	0.06	0.20	0.21	0.05
V_2O_3 (wt%)	0.09	0.09	0.01	0.23	0.24	0.04	0.20	0.18	0.08
Sc (mg/kg)	260	260	20	180	170	40	200	200	60
Total (wt%)	102.11	102.16	0.92	102.18	102.21	1.37	102.14	102.19	0.04

Table 5
LA-ICP-MS analysis of bauxite hematite matrix sites. Fe was used as a standard element. Therefore, its content appears constant in all the analyzed spots (see paragraph 2.). SiO_2 measurements are from SEM-EDS.

Analyte	Bauxite DD							Bauxite ST			
	1	2	3	4	5	6	7	8	9	Average	S.D.
Fe_2O_3 (wt%)	91.86	91.86	91.86	91.86	91.86	91.86	91.86	91.99	91.99	91.89	0.06
TiO_2 (wt%)	2.61	2.65	2.47	2.62	2.59	2.57	2.71	3.27	3.19	2.74	0.29
Al_2O_3 (wt%)	3.11	3.97	4.37	8.81	4.66	5.23	5.81	4.35	9.66	5.55	2.23
SiO_2 (wt%)	0.60	0.60	0.60	0.00	0.60	0.60	0.00	0.30	0.30	0.40	0.26
Cr_2O_3 (wt%)	0.25	0.26	0.25	0.30	0.26	0.25	0.27	0.33	0.37	0.28	0.04
V_2O_3 (wt%)	0.19	0.20	0.19	0.18	0.19	0.19	0.17	0.24	0.26	0.20	0.03
Sc (mg/kg)	220	220	214	204	214	209	205	146	157	199	28
Total (wt%)	98.62	99.54	99.74	103.77	100.15	100.70	100.82	100.48	105.76	101.06	2.26

6.2.2. Bauxite residue

As in bauxite samples the most commonly encountered Sc-containing particle type in its residues was hematite-dominant (Fig. 4). Two populations of hematite-dominant particles were categorized as Sc-hosting and Sc-depleted (Table 6). The population of Sc-depleted material (average 30 mg/kg) was defined by categorizing Sc concentrations below the lowest measured content of Sc in bauxite samples hematite matrices, < 100 mg/kg (Table A.3). This category is thought to represent material derived from lateritic bauxite feed, which has a negligible bulk Sc content (7–8.6 mg/kg). It is not possible to propose any other sources for this population of Sc-depleted hematite. The Sc-hosting category has a similar average Sc concentration (190 mg/kg, Table 6) as the examined population of Greek bauxite hematite matrices (200 mg/kg, Table 4). The bauxite feed proportion in the production is 80% karst and 20% lateritic and the hematite input is therefore 90% from karst and 10% lateritic bauxite (calculated by combining phase quantities in Table 3 and the feed proportions). This reasoning allows an overall estimation of average Sc content in hematite-dominant particles of bauxite residue to be reported as 170 mg/kg.

In the bauxite residue sample, another iron phase was distinguished

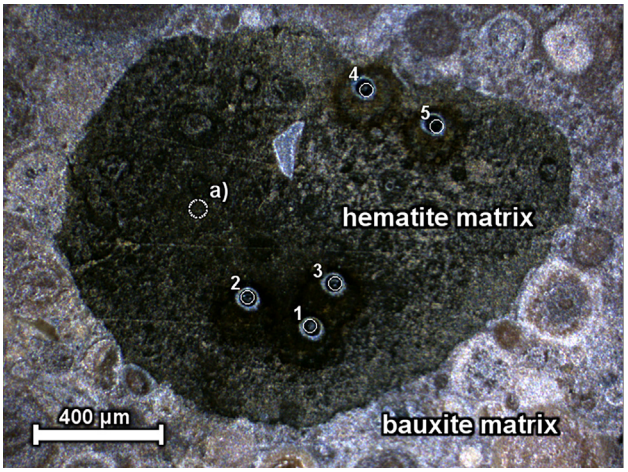

Fig. 2. Optical microscope image of bauxite DD hematite-dominant matrix area, surrounded by multiphase bauxite matrix. The numbers indicate LA-ICP-MS measurement spots (Table 5) and "a)" is the spot of µ-Raman measurement depicted in Fig. 3.

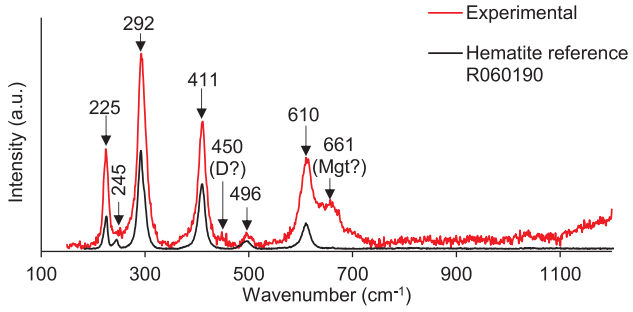

Fig. 3. Raman spectrum of an example hematite matrix area of bauxite DD in relation to hematite reference. D — diaspore, Mgt — magnetite. Peaks with only numeric indexing are attributed to hematite. Reference spectrum is from RRUFF database, reprinted with permission from RRUFF project representative (Lafuente et al., 2015).

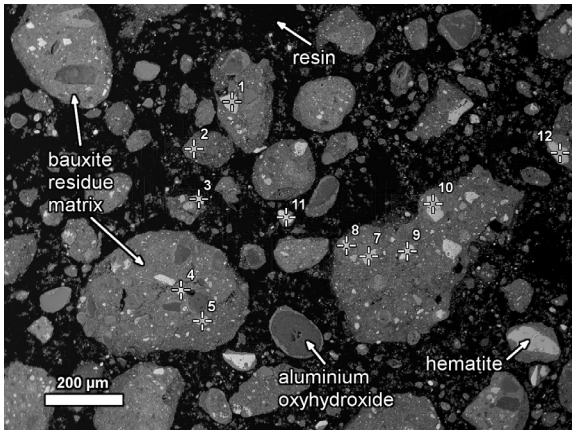

Fig. 4. Backscattered electron image of a selection of analyzed spots of hematite-dominant grains in bauxite residue. Measurements are summarized in Table 6 and individual measurements are reported in Table A.4.

from hematite by its darker hue in the backscattered electron imaging mode (Fig. 5) and its higher Sc content (Tables 6 and 7, and A.5). Quantitative EPMA-WDS analysis resulted in a deficiency of about 10% in total oxide values, and this is attributed to hydroxyl content. This iron oxyhydroxide phase was identified as goethite in µ-Raman spectroscopic analysis (bands 204, 221, 240, 296, 396, 472, 546 cm^{-1}), sometimes associated with hematite in the same particle (bands 224, 246, 291, 410, 495, 609 cm^{-1}) (Figs. 5 and 6) (De Faria et al., 1997; Lafuente et al., 2015). Raman identification of Sc-bearing goethite was repeated on several particles. The claimed goethite phase contains 330 mg/kg of Sc on average and maximum values exceed 800 mg/kg while the standard deviation is high because of the high spread of the measured values. Often, but not always, goethite is associated to Sc-depleted hematite containing no or very low amounts of Sc (Fig. 5, Table 7).

A potential scenario explaining the observed complex goethite/hematite structures as the one shown in Fig. 5 assumes that the mixed goethite/hematite particles originate from the lateritic bauxite instead of the karstic one and therefore are initially Sc-depleted. During the bauxite digestion stage, Sc might be partially dissolved from some Sc-bearing minerals into the Bayer process liquor and subsequently adsorbed on the goethite surface giving rise to goethite particles with high Sc concentration. The above hypothesis is not uncommon as Chassé et al. (2017) have revealed in a high Sc grade Australian laterite deposit that Sc is adsorbed on the surface of goethite, giving rise to an average concentration of about 1300 mg/kg associated with this phase. By contrast, in hematite Sc is held in the mineral lattice with a lower concentration of approximately 200 mg/kg (Chassé et al., 2017). In broad terms, a similar partitioning between hematite and goethite with regards to Sc contents is also evident in our investigated system of Bayer process derived residue. If this analogy holds true, the occurrence mode of Sc in goethite of present study could also be attributed to Sc adsorption phenomena.

Another scenario explaining the formation of complex goethite/hematite structures is based on the transformation of goethite to hematite that is induced through a reaction with lime. The reaction path includes the formation of iron hydrogarnet as an intermediate product which is further decomposed into hematite (Smith, 2017). During the transformation of the originally Sc-contained goethite phases to iron hydrogarnets, Sc is liberated because it cannot enter to the intermediate hydrogarnet phase, as indicated below (paragraph 3.4.2) and also reported in the literature (Suss et al., 2017), giving rise to the formation of a new Sc-depleted hematite phase.

6.3. Aluminum oxyhydroxides as minor scandium hosts

Diaspore and boehmite, the respective aluminum oxyhydroxide phases contained in bauxites as well as in the residues, are relatively depleted in Sc (Fig. 7, Table 8). As in the case of iron oxide matrices, we consider that the analyzed spots are not completely pure aluminum oxyhydroxides, but rather matrices of different phases with a high and prevailing content of Al_2O_3. Minor peaks of Sc could be identified on some of the qualitatively analyzed spots. The Sc amount that could be quantified was right on or slightly above the detection limit of EPMA-WDS method with an average of about 10 mg/kg (Table 8) in both bauxite (Table A.6) and bauxite residue aluminum oxyhydroxide particles (Table A.7). LA-ICP-MS measurements on the bauxite ST aluminum oxyhydroxide locations indicated an average of 16 mg/kg Sc (Table 9).

The results of this work prove once more the preference of Sc substitution towards iron phases instead of aluminum ones, due to the relative similarity of Sc^{3+} with Fe^{3+} rather than with Al^{3+}. The latter should not be excluded as the substitution of Al^{3+} by Sc^{3+} has also been described to take place (Horovitz, 1975) and in Middle Timan bauxite (Urals, Russia), this is the primary form of Sc occurrence (Suss et al., 2017). As a conclusion, a small proportion of Sc could possibly be released from diaspore/boehmite minerals to processing liquor during Bayer digestion.

Table 6
EPMA-WDS quantification of iron oxide matrices of bauxite residue.

Analyte	Sc-hosting hematite (n = 24)			Sc-depleted hematite (n = 32)			Goethite (n = 12)		
	Median	Average	S.D.	Median	Average	S.D.	Median	Average	S.D.
Fe_2O_3 (wt%)	93.55	92.02	4.06	93.93	93.81	3.49	84.86	85.89	4.84
TiO_2 (wt%)	3.52	3.98	2.17	0.94	1.02	0.82	0.72	2.36	3.34
Al_2O_3 (wt%)	1.82	1.79	0.60	1.66	1.91	1.47	0.61	0.75	0.72
SiO_2 (wt%)	0.45	0.71	0.60	1.14	1.11	0.68	1.76	1.84	0.43
Na_2O (wt%)	0.21	0.29	0.26	0.40	0.43	0.27	0.37	0.36	0.23
CaO (wt%)	0.42	0.49	0.32	0.42	0.44	0.17	0.20	0.29	0.20
Cr_2O_3 (wt%)	0.18	0.24	0.12	0.03	0.05	0.05	0.03	0.05	0.04
V_2O_3 (wt%)	0.14	0.17	0.11	0.03	0.07	0.12	0.04	0.05	0.03
Sc (mg/kg)	180	190	70	30	30	20	300	330	240
Total (wt%)	101.05	99.74	3.39	99.26	98.99	2.28	90.80	91.73	3.15

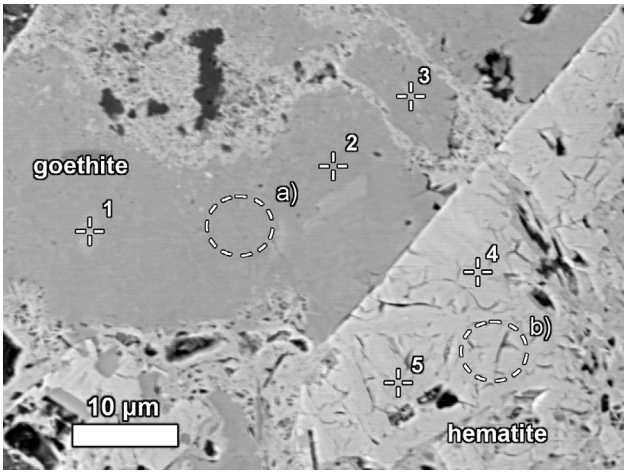

Fig. 5. Sc-rich goethite and Sc-depleted hematite contained in bauxite residue shown on backscattered electron image. Numbers 1 – 5 indicate to EPMA-WDS measurements (Table 7); letters "a)" and "b)" indicate the approximate areas of µ-Raman measurements (Fig. 6).

Table 7
EPMA-WDS quantification of goethite (1–3) and hematite (4–5) areas corresponding to Fig. 5.

Analyte	Goethite			Hematite	
	1	2	3	4	5
Fe_2O_3 (wt%)	88.91	80.13	83.07	101.11	100.80
TiO_2 (wt%)	0.33	7.81	9.33	1.56	1.52
Al_2O_3 (wt%)	0.15	0.51	0.69	0.11	0.15
SiO_2 (wt%)	1.70	1.39	1.59	0.07	0.10
Na_2O (wt%)	0.20	0.15	0.46	0.03	0.01
CaO (wt%)	0.14	0.10	0.17	0.10	0.13
Cr_2O_3 (wt%)	0.00	0.02	0.07	0.08	0.09
V_2O_3 (wt%)	0.01	0.08	0.11	0.28	0.28
Sc (mg/kg)	300	400	290	0	10
Total (wt%)	91.47	90.26	95.53	103.34	103.08

6.4. Minor and secondary phases

6.4.1. Sc-hosting

Zircon ($ZrSiO_4$), detected in bauxite and its residue samples, was found to contain the highest concentration of scandium throughout the analyzed mineral species with an average of about 3600 mg/kg (Table 10). In the observed grains, zones with higher Sc and Ca contents can be detected, visualized in backscattered electron imaging by darker tones (Fig. 8). Very high heterogeneity of Sc contents in zircon is evident, probably because of Sc-depleted zircons originating from lateritic bauxite and/or because of the zonation of the Sc presence in zircon.

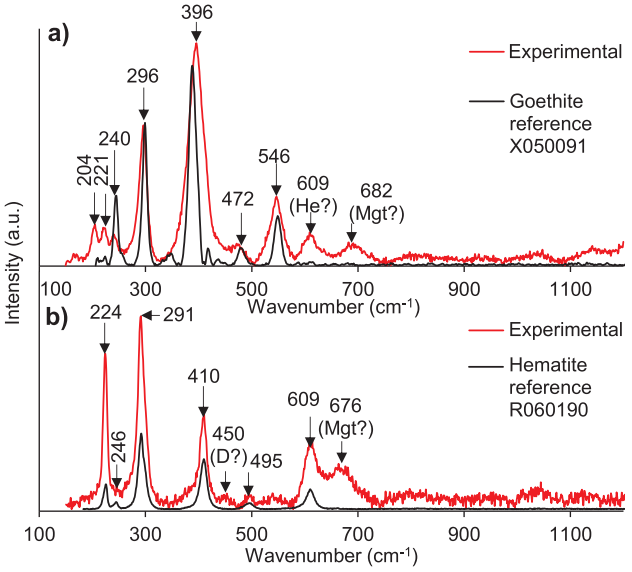

Fig. 6. Raman spectra of a) goethite area and b) hematite area contained in bauxite residue in relation to reference spectra. Analyzed locations are indicated on Fig. 5. He — hematite, D — diaspore, Mgt — magnetite; peaks with only numeric indexing are attributed to a) goethite, b) hematite. Reference spectra are from RRUFF database, reprinted with permission from RRUFF project representative (Lafuente et al., 2015).

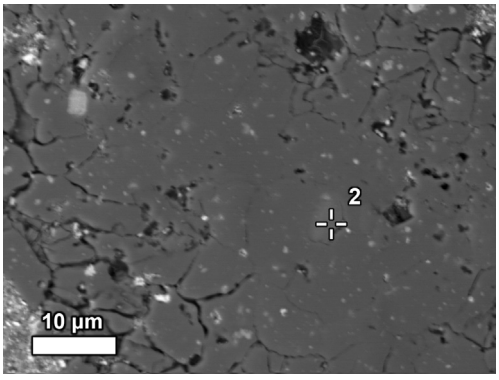

Fig. 7. Backscattered electron image of an aluminum oxyhydroxide dominant particle observed in bauxite residue. Quantification of spot "2" is shown in Table A.7.

This results also in a very high standard deviation. Sc bearing zircon, containing also Hf, U and Ca consistent with present observations, was detected in karst bauxite in the Southern Apennines, Italy (Boni et al., 2013). It seems that in bauxite residue, the highest values of Sc in zircon

Table 8
EPMA-WDS quantification of aluminum oxyhydroxide matrices of bauxite samples (n = 14).

Analyte	Median	Average	S.D.
Fe_2O_3 (wt%)	3.53	4.03	1.88
TiO_2 (wt%)	0.18	0.42	0.46
Al_2O_3 (wt%)	88.40	89.02	2.18
SiO_2 (wt%)	0.45	0.44	0.25
Na_2O (wt%)	0.01	0.01	0.01
CaO (wt%)	0.04	0.06	0.09
Sc (mg/kg)	10	10	10
Total (wt%)	94.87	93.98	2.91

are correlated with the higher concentrations of Ca, Al as well as U when comparing with the measurements with low Sc concentration. However, the Sc concentration does not seem to be dependent on Hf concentrations. Therefore, a multivalent substitution in zircon involving Ca, Al, U and Sc can be hypothesized to exist. The zonation of zircon with Sc-enriched areas has been explained to occur because of zircon alteration in some bauxite deposits, giving rise to a partly amorphized structure (Mordberg et al., 2001). In present case, we do not observe features indicating to alteration or amorphousness of zircon, but the morphology of the crystals rather indicates to fracturing and a subsequent filling of the fractures with Sc-enriched zircon. More insight into zircon occurrence in bauxite and its properties in relation to Sc content can be found from Mordberg et al. (2001). The Bayer process is expected to have no or minimum effect on zircon because of its well-known high chemical durability (e.g. Hanchar, 2015), which is also evident from current observations.

6.4.2. Sc-depleted

Titanium dioxide polymorphs anatase and/or rutile do not contain a significant amount of Sc (Table A.8). Anatase and rutile can't be distinguished from each other in EPMA-WDS because of their identical chemical composition (Fig. 9). The concentrations of Sc in titanium dioxides of bauxite and its residue materials were similar, a summarizing concentration of about 40 mg/kg (n = 9) can be given for the two phases combined. Iron titanates, corresponding to either ilmenite or titanomagnetite (not detected in XRD) showed variable contents of Sc from 0 to 260 mg/kg, but are commonly completely barren in Sc content (Fig. 9, Table A.9).

There are no indications suggesting to the existence of any discrete phases of Sc in bauxite or its residue. Rare earth element phases and aluminosilicate phases, latter corresponding to kaolinite group clay minerals, did not reveal any content of Sc. The chlorite group phase chamosite, detected in XRD scan of bauxite residue, was not discerned during EPMA investigation. Neither observation derived any conclusions about the relations between phosphates and Sc.

The Bayer process secondary minerals of the hydrogarnet group, cancrinite or perovskite did not detect the presence of Sc, when analyzing them in bauxite residue. Only a few small perovskite grains were possible to be analyzed in EPMA. Due to the very fine size of cancrinite and perovskite grains in bauxite residue, these phases were investigated on a sample of scale formed in the Bayer process autoclave (74% cancrinite, 7.5% perovskite, 6.5% hematite, 12% other; 19.7 mg/kg Sc; Tables 2 and 3). In this material, the crystals exhibit larger sizes while representing Bayer process secondary mineral phases (Fig. 10). Perovskite-dominant matrix did not detect any presence of Sc, while cancrinite-dominant matrix indicated 20–90 mg/kg of Sc (Table 11). There is a partial overlap in the WDS energy lines of Ca and Sc. To overcome that, the scale sample was additionally subjected to LA-ICP-MS measurements. It provided evidence for the same conclusion that perovskite and cancrinite are depleted in Sc, but still the detected quantities ranged from 12 to 37 mg/kg Sc on different spots. Unfortunately, the LA-ICP-MS spot size (40 μm) is larger than the individual perovskite crystals (about 5 μm), therefore a single crystal cannot be targeted with this experiment. The analyzed minerals (perovskite and cancrinite) might contain only a minor amount of Sc (< 30 mg/kg), as suggested by the bulk (Table 2) as well as spot Sc analysis (Table 11) of the scale sample, whereas cancrinite is a more probable host for Sc. However, the detected quantities can also be attributed to the presence of minute iron oxide particles in the scale sample (Fig. 10). To confirm whether cancrinite can incorporate Sc to its composition, a purer source of cancrinite phase should be isolated. In any case, even if cancrinite contains roughly about 30 mg/kg of Sc, it cannot account for more than 3% of the total Sc inventory in bauxite residue, rendering its importance as a Sc host to be minimum. Note that other minor and trace elements such as Mg, Cr V and Ni are significantly enriched into the perovskite-dominant matrix compared to cancrinite matrix (Table 11). This indicates that Bayer process scales can be studied to elucidate the relations of trace elements with Bayer process specific mineral phases.

6.5. Distribution of scandium between its host minerals

Having quantified the phase compositions (Table 3), Sc bulk concentrations (Table 2) and the contents in its host minerals (Sections 6.2, 6.3 and 6.4.1), we can compile the data into a mass balance estimation to indicate the amount of the total Sc each phase contains. Higher and lower limits are determined by the standard deviations of Sc quantification. The estimation is based on EPMA-EDS data, values of major phases are rounded to a multiple of 5. For the bauxite residue, the most significant Sc host is hematite, containing 55 ± 20% of total Sc, followed by goethite with 25 ± 20% of contribution (Table 12). A lesser amount is associated with zircon and we can estimate a quantity of 10 ± 5% Sc hosted by this mineral. The primary change from bauxite to bauxite residue is that boehmite/diaspore lose their role of hosting Sc, because they are dissolved in the Bayer process (e.g. Authier-Martin et al., 2001). Other authors have arrived at the same conclusion, that some Sc is released from diaspore/boehmite, but in their case the boehmite/diaspore-associated proportion of Sc in bauxite is reportedly substantially higher (100–110 mg/kg Sc; 55–60% of total Sc) than in present case (Suss et al., 2017). The released proportion of Sc could be scattered in bauxite residue in the form of adsorbed ions on mineral surfaces or on the goethite surface. Goethite was not distinctively observed in bauxite samples and the presence of Sc in them could not be identified. Therefore, goethite related mass balance figure can only be

Table 9
LA-ICP-MS quantification of aluminum oxyhydroxide matrices of bauxite ST. Al was used as a standard element. SiO_2 is from SEM-EDS.

Analyte	1	2	3	4	5	6	7	Average	S.D.
Fe_2O_3 (wt%)	2.52	2.66	3.21	2.43	3.15	3.22	3.51	2.96	0.42
TiO_2 (wt%)	1.91	1.82	1.86	1.53	0.11	0.12	0.13	1.07	0.89
Al_2O_3 (wt%)	82.14	82.13	82.13	82.13	81.38	82.51	82.51	82.13	0.38
SiO_2 (wt%)	0.00	0.00	0.00	0.00	1.07	0.86	0.86	0.40	0.50
Cr_2O_3 (wt%)	0.02	0.02	0.02	0.02	0.01	0.01	0.02	0.02	0.00
V_2O_3 (wt%)	0.04	0.04	0.05	0.05	0.03	0.03	0.03	0.04	0.01
Sc (mg/kg)	23	20	20	15	10	10	11	16	6
Total (wt%)	86.68	86.74	87.33	86.20	85.79	86.78	87.09	86.66	0.52

Table 10
Sc contents in zircons of bauxite (1–4) and its residue (5–10), quantified in EPMA-WDS.[a]

Ana-lyte	Bauxites ST and DD				Bauxite residue							
	1	2	3	4	5	6	7	8	9	10	Ave-rage	S.D.
ZrO_2 (wt%)	56.80	59.02	55.06	61.10	56.53	61.82	57.73	57.98	62.52	57.45	58.60	2.46
SiO_2 (wt%)	24.78	26.01	30.20	31.86	30.07	32.65	30.37	30.53	32.70	30.23	29.94	2.61
Fe_2O_3 (wt%)	3.82	3.05	4.30	3.20	3.97	3.52	4.10	3.95	3.27	3.98	3.72	0.43
HfO_2 (wt%)	n/a	n/a	n/a	n/a	1.14	1.48	1.14	1.15	1.50	1.16	1.26	0.18
CaO (wt%)	0.50	0.02	0.42	0.02	0.64	0.00	0.54	0.65	0.01	0.69	0.35	0.30
UO_2 (wt%)	n/a	n/a	n/a	n/a	0.82	0.33	0.79	0.86	0.21	0.87	0.65	0.29
Al_2O_3 (wt%)	n/a	n/a	n/a	n/a	n/a	n/a	n/a	0.72	0.02	0.82	0.52	0.44
Sc (mg/kg)	1860	350	3100	540	7240	80	7180	7230	50	8400	3600	3500
Total (wt%)	86.20	88.14	90.45	96.27	94.28	99.82	95.77	96.94	100.24	96.48	94.46	4.73

[a] For a part of the measurements, Al_2O_3, HfO_2 and UO_2 contents were overlooked, but for a wider overview of Sc contents in zircon, these measurements were included as a part of this summary.

given for bauxite residue.

6.6. The route of scandium enrichment into bauxite residue

There are two main parent lithologies from where Parnassos-Ghiona bauxite material is thought to originate. First are the ultramafic and mafic rocks. They are linked to the bauxite deposit primarily by relating the contents of chromium and chromite mineral species as well as other compatible elements (Gamaletsos et al., 2016a; Laskou, 2001; Valeton et al., 1987). Second are felsic rocks of igneous origin, linked to the bauxite deposit by the elevated content of REEs and incompatible elements of the high field strength elements group (e.g. Th) as well as the presence of detrital zircon (Gamaletsos et al., 2016a; Valeton et al., 1987). Scandium source in the analyzed system can be assumed to be associated with the mafic and ultramafic rocks rather than the felsic ones because of the known relative abundance of Sc in mafic types of rocks (Jaireth et al., 2014; Samson and Chassé, 2016). The proportion of Sc reporting to zircon could be originating from the felsic rocks.

During source rock weathering, Sc^{3+} is released from its initial host minerals. Sc then often follows the behavior of Fe^{3+} because of the similarities in the Eh-pH stability field of hematite and Sc_2O_3 (Brookins, 1988; Hoatson et al., 2011; Jaireth et al., 2014). Furthermore, the ionic radii of six-coordinated Sc^{3+} and Fe^{3+} are similar, but still different enough to limit the maximum amount of Sc entering to hematite lattice (Chassé et al., 2017). Sc^{3+} and Fe^{3+} isomorphous substitution is a common scenario in various lithologies (Samson and Chassé, 2016) and expected also in present case.

During the Bayer process, the concentration of Sc in bauxite residue compared to material feed is further increased by a factor of 2.37, achieving its maximum concentration in the investigated system in AoG (Ochsenkühn-Petropulu et al., 1994; Vind et al., 2018), while the mineralogical occurrence remains practically the same as in bauxite.

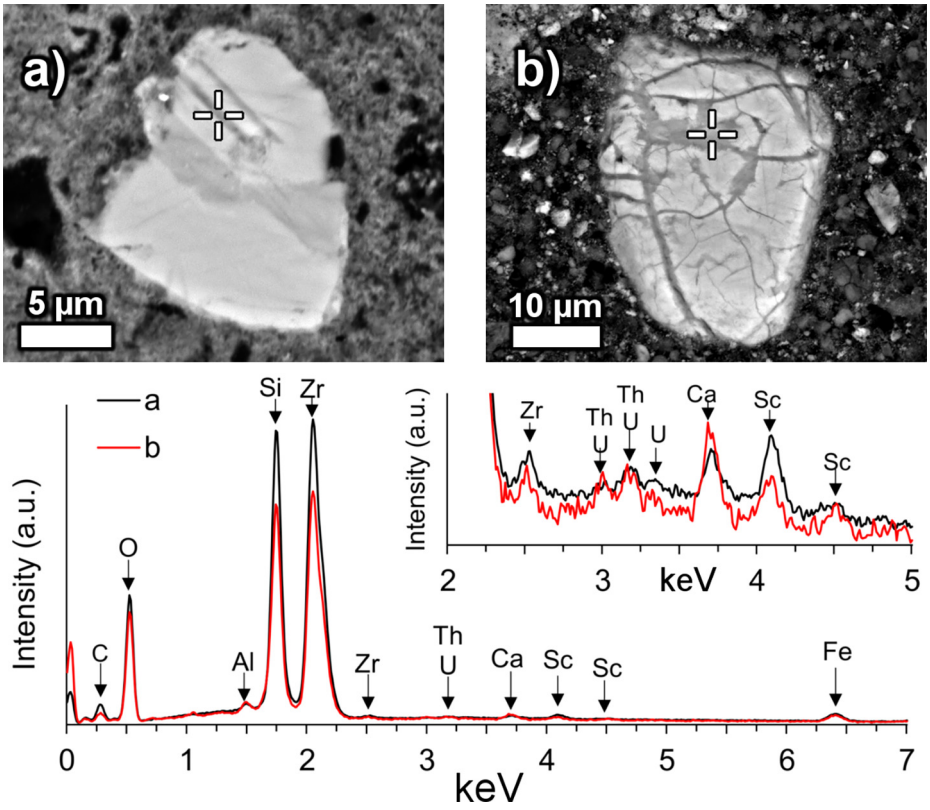

Fig. 8. Backscattered electron images of zircons observed in (a) Greek bauxite DD and (b) bauxite residue with respective EDS spectra.

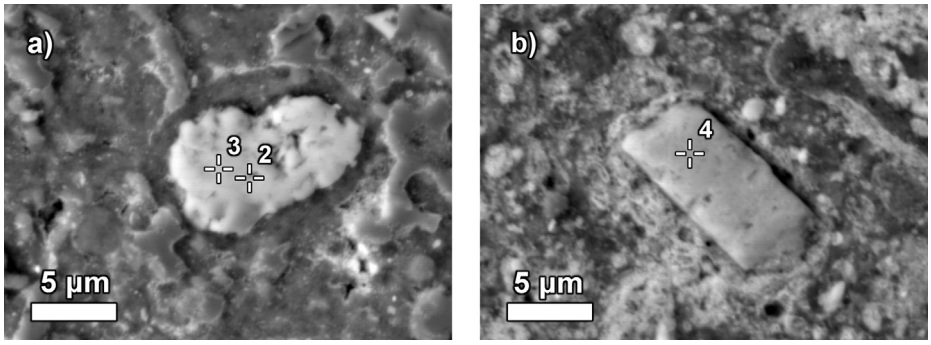

Fig. 9. Backscattered electron images of (a) titanium dioxide (anatase/rutile) and (b) iron titanate observed in Greek bauxite DD. The indicated quantification spots are reflected in (a) Table A.8 and (b) Table A.9.

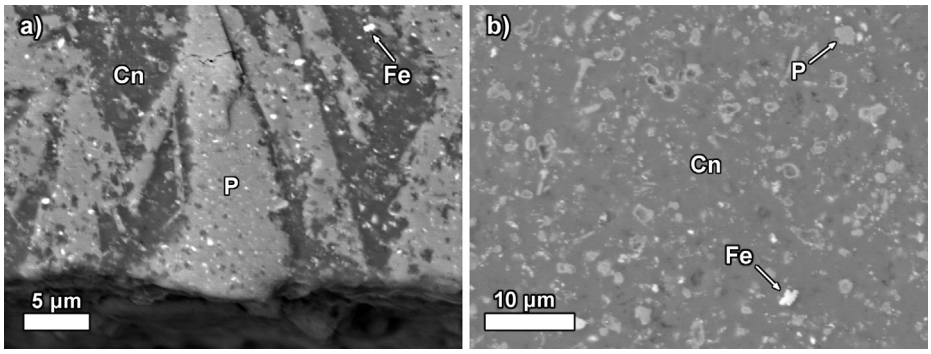

Fig. 10. Backscattered electron images of the Bayer process autoclave scale: (a) perovskite-enriched matrix, and (b) cancrinite-enriched matrix. Annotations: "P" — perovskite matrix, "Cn" — cancrinite matrix, "Fe" — iron oxide particle.

Table 11
Sc contents in perovskite-dominant (1–3) and cancrinite-dominant (4–5) matrices of digester autoclave scale, quantified in EPMA-WDS.

Analyte	Perovskite-dominant			Cancrinite-dominant	
	1	2	3	4	5
Fe_2O_3 (wt%)	9.69	10.18	9.30	2.30	4.41
TiO_2 (wt%)	34.39	30.71	36.19	0.55	2.19
Al_2O_3 (wt%)	14.18	15.83	13.21	34.72	28.30
SiO_2 (wt%)	1.61	2.07	0.84	22.54	19.62
Na_2O (wt%)	2.07	1.97	1.72	12.84	18.42
CaO (wt%)	17.83	16.81	18.05	1.35	3.61
MgO (wt%)	2.26	1.95	2.34	0.00	0.05
K_2O (wt%)	0.04	0.07	0.05	0.40	0.52
Cr_2O_3 (wt%)	0.256	0.220	0.211	0.031	0.036
V_2O_3 (wt%)	0.186	0.128	0.130	0.025	0.031
NiO (wt%)	0.619	0.565	0.630	0.052	0.038
Sc (mg/kg)	0	0	0	90	20
Total (wt%)	83.13	80.50	82.67	74.80	77.23

Table 12
Distribution of Sc between its host minerals. Titanium phases refer to anatase and rutile combined.

Phase	Bauxite	Bauxite residue
	% of total Sc	
Hematite	70 ± 20	55 ± 20
Goethite	?	25 ± 20
Diaspore/boehmite	15 ± 15	2 ± 2
Zircon	10 ± 5	10 ± 5
Titanium phases	2 ± 2	1 ± 1
Other/unaccounted	3	7

6.7. Linkages between the scandium occurrences and its leaching behavior

As already mentioned in the Introduction (paragraph 1), several experimental studies have been carried out for exploring the opportunities of recovering Sc from bauxite residue (Akcil et al., 2017; Borra et al., 2016; Davris et al., 2017; Zhang et al., 2016).

Borra et al. (2015) reported that during mineral acid leaching of bauxite residue, recovering 30–40% of Sc results in the leaching of only a minor part of Fe whereas recovering more than 50% of Sc unavoidably results in the dissolution of a major part of Fe. From the leaching correlation curves, they proposed that Sc is not homogeneously distributed between the iron oxide phases. Eventually, the recovery of Sc does not exceed 80% (Borra et al., 2015). During functionalized hydrophobic ionic liquid leaching of bauxite residue, Sc recovery reaches up to 45% while less than 3% of Fe is leached (Davris et al., 2016). The former examples agree with the conclusion of the present assessment that Sc is distributed mainly between goethite and hematite. The more easily leachable proportion of Sc (30–40%) is probably associated with goethite. Recovering the proportion of Sc that is accompanied with leaching a major part of Fe is most likely concentrated in the mineral lattice of hematite. The remaining part of Sc (~20%) that is resistant to leaching is presumably associated with the chemically durable zircon mineral.

On the other hand, over 50% of zirconium (Zr) recovery has been reported during 0.6 M H_2SO_4 leaching of AoG's bauxite residue. It was accompanied by 55% of Sc and only 3% of Fe recovery (Lymperopoulou et al., 2017). Therefore, it is possible that some leaching conditions also liberate Sc from zircon. The limiting factor for drawing any further conclusions is that Zr recovery has been reported only a very few times in the literature. We suggest that future studies should take into consideration to also analyze this parameter in the leachates to confirm the fate of zircon during the recovery of Sc from bauxite residue.

Indications to the correlating leaching behavior of Sc and Ti with regards to AoG's bauxite residue (Bonomi et al., 2017b; Ochsenkühn-

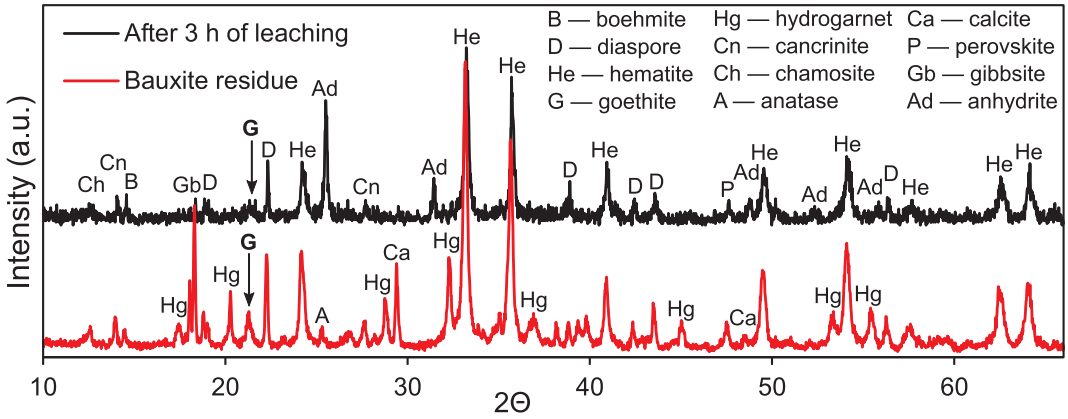

Fig. 11. Diffractogram of raw bauxite residue compared to diffractogram of residue after 3 h of leaching.

Petropulu et al., 1994; Rivera et al., 2017) did not acquire any mineralogical support in the context of present work. Only about 1% of total Sc could be found in titanium dioxides contained in bauxite residue.

Hereby we provide further evidences of Sc leaching behavior during an imidazolium ionic liquid [Emim][HSO_4] leaching of bauxite residue (Bonomi et al., 2017a, 2017b). After 3 h of leaching at 150 °C, about 31% of Sc and 7% of Fe were recovered. It can be observed from the diffractogram of leaching residues, that the first Sc-bearing phase to be almost dissolved is goethite, when compared to raw bauxite residue (Fig. 11). At the same time, practically all the hematite has remained in the residues. This supports the hypothesis that the easily extractable proportion of Sc in bauxite residue is associated with goethite phase. As already explained before, Sc concentration associated with goethite is substantially higher than the hematite-bound Sc (Section 6.2.2, Fig. 5, Tables 6 and 7). Other phases leached during the early stages of the experiment are gibbsite, calcite and hydrogarnet, but Sc is not found in these phases. The newly formed phase is anhydrite ($CaSO_4$). Maximum recovery of Sc, 78%, is achieved at 200 °C together with the complete dissolution of Fe, indicating to the major part of Fe occurring in hematite. Once again, the remaining unrecovered Sc is possibly fixed in zircon.

7. Conclusions

The present work sets a first benchmark in characterizing the modes of Sc occurrences in European bauxite residue on the example of materials from Aluminium of Greece. The close association of iron phases and Sc in bauxite and its residue, as indicated by previous authors, has been clearly confirmed. The claim was complemented with the quantification of Sc in its host minerals. Confirmed distinction of goethite hosting appreciable amount of Sc in addition to hematite was made. The average Sc concentration in the hematite matrix of the analyzed Greek Parnassos-Ghiona bauxite samples is 200 mg/kg and in the hematite matrix of AoG's bauxite residue it is 170 mg/kg. The latter is due to the dilution effect of Sc-depleted lateritic bauxite feed in the production flowsheet of AoG. In bauxite residue, hematite hosts 55 ± 20% of total Sc while goethite accounts for about 25 ± 20% of total Sc. Zircon hosts about 10 ± 5% of the total Sc in bauxite residue.

The probable Sc occurrence mode in hematite is the isomorphous substitution of Sc^{3+} and Fe^{3+}. Goethite assumes to host adsorbed Sc^{3+} cations on its particles surface, but this hypothesis needs further investigation. Minor hosts of Sc are titanium dioxides and aluminum oxyhydroxides, the latter represented by diaspore and boehmite. Since diaspore and boehmite are digested in the Bayer process, about 10% of Sc contained in them could be released from their lattice and transferred through surface adsorption to goethite of bauxite residue. The rest of the mineral phases in bauxite and bauxite residue system are generally not associated with Sc.

Sc concentrations in the main mineral matrices were cross-checked using two methods, EPMA-WDS and LA-ICP-MS and the quantification results of the two methods were in excellent agreement. It is evident that Sc occurs in different forms in different bauxites and their residues. It is necessary to investigate the nature of Sc occurrence in various materials case-by-case.

New evidence of Sc leaching behavior from bauxite residue shows that Sc is first released from goethite, then from hematite and the unrecovered proportion of Sc is likely associated with zircon.

The characterization of Sc in worldwide bauxite inventory deserves thorough geochemical surveying, because the literature review revealed the relative scarcity of information. The thorough understanding of the characteristics of Sc in bauxite deposits is crucial, because a large proportion of this valuable metal with an increasing demand on the market is thought to be associated with bauxites. Further work is encouraged to characterize Sc in the < 1 μm fraction of bauxite residue. Also, it could be of high interest to speciate further the properties of Sc in bauxite and its residue by performing advanced analyses such as the X-ray absorption near-edge structure (XANES) spectroscopy, synchrotron beamline μXRF and μXRD as well as nano-SIMS methods.

Acknowledgements

We thank Apostolos Kourtis from the National Technical University of Athens for his help with Raman microscopy. We are grateful for the help of György Bánvölgyi and Ken Evans who provided numerous comments and helped to correct the manuscript. Two anonymous reviewers are acknowledged for helping to improve the manuscript. The research leading to these results has received funding from the European Community's Horizon 2020 Programme (H2020/2014–2019) under Grant Agreement no. 636876 (MSCA-ETN REDMUD). This publication reflects only the authors' views, exempting the Community from any liability. Project website: http://www.etn.redmud.org. Conflicts of interest: none.

Appendix A. Supplementary material

Supplementary data associated with this article can be found, in the online version, at http://dx.doi.org/10.1016/j.mineng.2018.04.025.

References

Adamson, A.N., Bloore, E.J., Carr, A.R., 2013. Basic Principles of Bayer Process Design. In: Donaldson, D., Raahauge, B.E. (Eds.), Reprinted in Essential Readings in Light Metals. John Wiley & Sons Inc, pp. 100–117 (2013).

Akcil, A., Akhmadiyeva, N., Abdulvaliyev, R., Meshram Abhilash, P., 2017. Overview on extraction and separation of rare earth elements from red mud: focus on scandium. Miner. Process. Extr. Metall. Rev. 1–7. http://dx.doi.org/10.1080/08827508.2017.1288116.

Alkan, G., Xakalashe, B., Yagmurlu, B., Kaussen, F., Friedrich, B., 2017. Conditioning of

red mud for subsequent titanium and scandium recovery — a conceptual design study. World Metall. – Erzmetall 70, pp. 5–12.
Anagnostou, C., 2010. Bauxite resource exploitation in Greece vs sustainability, in: Bulletin of the Geological Society of Greece. Presented at the 12th International Congress of The Geological Society of Greece. Planet Earth: Geological Processes And Sustainable Development, Patras, Greece, 19-22 May 2010, pp. 2425–2436.
Authier-Martin, M., Forte, G., Ostap, S., See, J., 2001. The mineralogy of bauxite for producing smelter-grade alumina. JOM 53, 36–40. http://dx.doi.org/10.1007/s11837-001-0011-1.
Balomenos, E., Giannopoulou, I., Panias, D., Paspaliaris, I., 2009. ENEXAL: Novel technologies for enhanced energy and exergy efficiencies in primary aluminium production industry. MJoM 15, 203–217.
Bánvölgyi, G., 2016. Scale formation in alumina refineries. In: Proceedings of the 34th International Conference and Exhibition ICSOBA, Travaux 45. Quebec, Canada, 3-6 October, pp. 1–14.
Bárdossy, G., 1982. Karst bauxites: bauxite deposits on carbonate rocks, Developments in Economic Geology 14. Elsevier Scientific Pub. Co., Amsterdam, Netherlands.
Bárdossy, G., Pantó, G., 1973. Trace mineral and element investigation in bauxites by electron-probe. In: Proceedings. Presented at the 3rd International Congress of ICSOBA, Academie des Sciences de Hongrie, Nice, France, 17-21 September 1973, pp. 47–53.
Binnemans, K., Jones, P.T., Blanpain, B., Van Gerven, T., Pontikes, Y., 2015. Towards zero-waste valorisation of rare-earth-containing industrial process residues: a critical review. J. Clean. Prod. 99, 17–38. http://dx.doi.org/10.1016/j.jclepro.2015.02.089.
Blankova, T.N., Kalinin, A.I., Kalinina, N.E., Khamatdinova, G.S., 1977. Neutron-activation analysis of bauxites and products of their processing. J. Radioanal. Chem. 38, 341–349. http://dx.doi.org/10.1007/BF02520211.
Boni, M., Rollinson, G., Mondillo, N., Balassone, G., Santoro, L., 2013. Quantitative mineralogical characterization of karst bauxite deposits in the southern Apennines, Italy. Econ. Geol. 108, 813–833. http://dx.doi.org/10.2113/econgeo.108.4.813.
Bonomi, C., Davris, P., Balomenos, E., Giannopoulou, I., Panias, D., 2017. Ionometallurgical leaching process of bauxite residue: a comparison between hydrophilic and hydrophobic ionic liquids. In: Proceedings, Travaux 46. Presented at the 35th International ICSOBA Conference, ICSOBA, Hamburg, Germany, 2-5 October 2017, pp. 557–564.
Bonomi, C., Giannopoulou, I., Panias, D., 2017. Correlation of scandium and titanium during leaching of bauxite residue (red mud) by an imidazolium ionic liquid. In: Balomenos, E., Marinos, D. (Eds.), Book of Abstracts. Presented at the 2nd Conference on European Rare Earth Resources, Heliotopos Conferences Ltd., Santorini, Greece, 28-31 May 2017, pp. 182–184.
Borra, C.R., Blanpain, B., Pontikes, Y., Binnemans, K., Van Gerven, T., 2016. Recovery of rare earths and other valuable metals from bauxite residue (red mud): a review. J. Sustain. Metall. 2, 365–386. http://dx.doi.org/10.1007/s40831-016-0068-2.
Borra, C.R., Pontikes, Y., Binnemans, K., Van Gerven, T., 2015. Leaching of rare earths from bauxite residue (red mud). Miner. Eng. 76, 20–27. http://dx.doi.org/10.1016/j.mineng.2015.01.005.
Breiter, K., Förster, H.-J., Škoda, R., 2006. Extreme P-, Bi-, Nb-, Sc-, U- and F-rich zircon from fractionated perphosphorous granites: The peraluminous Podlesí granite system, Czech Republic. Lithos, Compositional Variation in Metamorphic Accessory Phases 88, 15–34. http://dx.doi.org/10.1016/j.lithos.2005.08.011.
Brookins, D.G., 1988. Eh-pH Diagrams for Geochemistry. Springer Science & Business Media, ISBN 978-3-642-73093-1, Berlin, Germany.
Chassé, M., Griffin, W.L., O'Reilly, S.Y., Calas, G., 2017. Scandium speciation in a world-class lateritic deposit. Geochem. Perspect. Lett. 105–114. http://dx.doi.org/10.7185/geochemlet.1711.
Chin, L.A.D., 1988. The state-of-the-art in Bayer process technology. In: Proceedings. Presented at the TMS Annual Meeting, TMS, Phoenix, USA, 25–28 January 1988, pp. 49–53.
Das, H.A., Zonderhuis, J., van der Marel, H.W., 1971. Scandium in rocks, minerals and sediments and its relations to iron and aluminium. Contrib. Mineral. Petrol. 32, 231–244. http://dx.doi.org/10.1007/BF00643336.
Davris, P., Balomenos, E., Panias, D., Paspaliaris, I., 2016. Selective leaching of rare earth elements from bauxite residue (red mud), using a functionalized hydrophobic ionic liquid. Hydrometallurgy 164, 125–135. http://dx.doi.org/10.1016/j.hydromet.2016.06.012.
Davris, P., Balomenos, E., Panias, D., Paspaliaris, I., 2014. Leaching of rare earths from bauxite residues using imidazolium based ionic liquids. In: Book of Proceedings. Presented at the ERES2014: 1st European Rare Earth Resources Conference, Heliotopos Conferences Ltd., Milos, Greece, 4-7 September 2014, pp. 241–251.
Davris, P., Balomenos, E., Taxiarchou, M., Panias, D., Paspaliaris, I., 2017. Current and alternative routes in the production of rare earth elements. BHM Berg- Hüttenmänn. Monatshefte 162, 245–251. http://dx.doi.org/10.1007/s00501-017-0610-y.
De Faria, D.L.A., Venâncio Silva, S., Oliveira, M.T., 1997. Raman microspectroscopy of some iron oxides and oxyhydroxides. J. Raman Spectrosc. 28, 873–878. http://dx.doi.org/10.1002/(SICI)1097-4555(199711)28:11<873::AID-JRS177>3.0.CO;2-B.
Deady, É.A., Mouchos, E., Goodenough, K., Williamson, B.J., Wall, F., 2016. A review of the potential for rare-earth element resources from European red muds: examples from Seydişehir, Turkey and Parnassus-Giona, Greece. Mineral. Mag. 80, 43–61. http://dx.doi.org/10.1180/minmag.2016.080.052.
Derevyankin, V.A., Porotnikova, T.P., Kocherova, E.K., Yumasheva, I.V., Moiseev, V.E., 1981. Behaviour of scandium and lanthanum in the production of alumina from bauxite (*in Russian*). Izv. Vysshikh Uchebnykh Zaved. Tsvetnaya Metall. 86–89.
European Commission, Deloitte Sustainability, TNO, British Geological Survey, Bureau de Recherches Géologiques et Minières, 2017. Study on the review of the list of critical raw materials. Publications Office of the European Union, Luxembourg, 1–93. doi: 10.2873/876644.
Evans, K., 2016. The history, challenges, and new developments in the management and use of bauxite residue. J. Sustain. Metall. 2, 316–331. http://dx.doi.org/10.1007/s40831-016-0060-x.
Feret, F.R., See, J., 2010. A comparative study of analytical methods of trace elements in bauxite and red mud. In: Proceedings of the 18th International Symposium ICSOBA Travaux, No. 35. Presented at the 18th International Symposium ICSOBA, Zhengzhou, China, 25-28 November, pp. 68–83.
Gamaletsos, P., Godelitsas, A., Chatzitheodoridis, E., Kostopoulos, D., 2007. Laser μ-Raman investigation of Greek bauxites from the Parnassos-Ghiona active mining area. In: Bulletin of the Geological Society of Greece. Presented at the 11th International Conference of the Geological Society of Greece: "Geoenvironment – Past – Present – Future," Athens, Greece, 24-26 May 2007, pp. 736–746.
Gamaletsos, P., Godelitsas, A., Kasama, T., Goettlicher, J., Steininger, R., 2016. Nano-mineralogy & -geochemistry of karst bauxites (Greece): Implications of the origin of the deposits. In: Goldschmidt Conference Abstracts. Presented at the V.M. Goldschmidt Conference, Yokohama, Japan, 27 June - 1 July 2016, pp. 894–894.
Gamaletsos, P.N., Godelitsas, A., Kasama, T., Church, N.S., Douvalis, A.P., Göttlicher, J., Steininger, R., Boubnov, A., Pontikes, Y., Tzamos, E., Bakas, T., Filippidis, A., 2017. Nano-mineralogy and -geochemistry of high-grade diasporic karst-type bauxite from Parnassos-Ghiona mines, Greece. Ore Geol. Rev. 84, 228–244. http://dx.doi.org/10.1016/j.oregeorev.2016.11.009.
Gamaletsos, P.N., Godelitsas, A., Kasama, T., Kuzmin, A., Lagos, M., Mertzimekis, T.J., Göttlicher, J., Steininger, R., Xanthos, S., Pontikes, Y., Angelopoulos, G.N., Zarkadas, C., Komelkov, A., Tzamos, E., Filippidis, A., 2016b. The role of nano-perovskite in the negligible thorium release in seawater from Greek bauxite residue (red mud). Sci. Rep. 6, 1–13. http://dx.doi.org/10.1038/srep21737.
Gambogi, J., 2017. USGS Minerals Information: Scandium [WWW Document]. URL https://minerals.usgs.gov/minerals/pubs/commodity/scandium/ (accessed 9.18.17).
Gräfe, M., Klauber, C., 2011. Bauxite residue issues: IV. Old obstacles and new pathways for in situ residue bioremediation. Hydrometallurgy 108, 46–59. http://dx.doi.org/10.1016/j.hydromet.2011.02.005.
Gu, H., Wang, N., Yang, Y., Zhao, C., Cui, S., 2016. Features of distribution of uranium and thorium in red mud. Physicochem. Probl. Miner. Process. 53, 110–121. http://dx.doi.org/10.5277/ppmp170109.
Hanchar, J.M., 2015. Zircon. In: Rink, W.J., Thompson, J.W. (Eds.), Encyclopedia of Scientific Dating Methods, Encyclopedia of Earth Sciences Series. Springer, Netherlands, pp. 959–962. http://dx.doi.org/10.1007/978-94-007-6304-3_58.
Hertel, T., Blanpain, B., Pontikes, Y., 2016. A Proposal for a 100 % use of bauxite residue towards inorganic polymer mortar. J. Sustain. Metall. 2, 394–404. http://dx.doi.org/10.1007/s40831-016-0080-6.
Hoatson, D.M., Jaireth, S., Miezitis, Y., 2011. The major rare-earth-element deposits of Australia: Geological setting, exploration and resources. Technical report, Australian Government, Geoscience Australia, ISBN 978–1–921954–02–3 http://www.ga.gov.au/corporate_data/71820/Complete_Report.pdf.
Horovitz, C.T., 1975. Scandium — its Occurrence, Chemistry, Physics, Metallurgy, Biology and Technology. Academic Press, London, Great Britain.
Jaireth, S., Hoatson, D.M., Miezitis, Y., 2014. Geological setting and resources of the major rare-earth-element deposits in Australia. Ore Geol. Rev. 62, 72–128. http://dx.doi.org/10.1016/j.oregeorev.2014.02.008.
Kawashima, N., Shi, L., Xu, N., Li, J., Gerson, A.R., 2016. Characterisation of single-stream Bayer plant heat exchanger scale. Hydrometallurgy 159, 75–86. http://dx.doi.org/10.1016/j.hydromet.2015.10.025.
Lafuente, B., Downs, R.T., Yang, H., Stone, N., 2015. The power of databases: The RRUFF project. DE GRUYTER, Berlin, München, Boston, pp. 1–30. http://dx.doi.org/10.1515/9783110417104-003.
Laskou, M., 2001. Chromite in karst bauxites, bauxitic laterites and bauxitic clays of Greece. In: Piestrzynski et al. (Ed.), Mineral Deposits at the Beginning of the 21st Century. Presented at the 6th Biennial SGS Meeting, Swets & Zeitlinger Publishers Lisse, Krakow, Poland, 26-29 August 2001, pp. 1091–1094.
Laskou, M., 1991. Concentrations of rare earths in Greek bauxites. Acta Geol. Hung. 34, 395–404.
Laskou, M., Economou-Eliopoulos, M., 2013. Bio-mineralization and potential biogeochemical processes in bauxite deposits: genetic and ore quality significance. Mineral. Petrol. 107, 471–486. http://dx.doi.org/10.1007/s00710-012-0257-z.
Laskou, M., Economou-Eliopoulos, M., 2007. The role of microorganisms on the mineralogical and geochemical characteristics of the Parnassos-Ghiona bauxite deposits, Greece. J. Geochem. Explor. 93, 67–77. http://dx.doi.org/10.1016/j.gexplo.2006.08.014.
Lavalou, E., Bosca, B., Keramidas, O., 1999. Alumina production from diasporic bauxites. Light Met. 55–62.
Lavrenchuk, V.N., Stryapkov, A.V., Kokovin, E.N., 2004. Scandium in bauxite and clay. GUP SO Kamensk-Uralsk Printshop.
Liu, Z., Li, H., 2015. Metallurgical process for valuable elements recovery from red mud—A review. Hydrometallurgy 155, 29–43. http://dx.doi.org/10.1016/j.hydromet.2015.03.018.
Lymperopoulou, T., Tsakanika, L.-A., Ochsenkühn, K.-M., Ochsenkühn-Petropoulou, M., 2017. Optimization of mineral acids leaching process for the recovery of rare earth elements from Greek red mud. In: Book of Abstracts. Presented at the 2nd Conference on European Rare Earth Resources, Heliotopos Conferences Ltd., Santorini, Greece, 28-31 May 2017, pp. 182–184.
Menges, F., 2017. Spectragryph - optical spectroscopy software version 1.0.7. Universität Konstanz, Obersdorf, Germany.
Mettos, A., Rondoyanni, T., Ioakim, C., 2008. Reconsideration of the structural relationship between the Parnassus-Ghiona and Vardoussia geotectonic zones in central Greece. Int. J. Earth Sci. 98, 1927–1934. http://dx.doi.org/10.1007/s00531-008-

0350-z.
Mongelli, G., Boni, M., Oggiano, G., Mameli, P., Sinisi, R., Buccione, R., Mondillo, N., 2017. Critical metals distribution in Tethyan karst bauxite: The cretaceous Italian ores. Ore. Geol. Rev. 86, 526–536. http://dx.doi.org/10.1016/j.oregeorev.2017.03.017.
Mordberg, L.E., Stanley, C.J., Germann, K., 2001. Mineralogy and geochemistry of trace elements in bauxites: the Devonian Schugorsk deposit, Russia. Mineral. Mag. 65, 81–101.
Ochsenkühn-Petropulu, M., Lyberopulu, T., Parissakis, G., 1994. Direct determination of lanthanides, yttrium and scandium in bauxites and red mud from alumina production. Anal. Chim. Acta 296, 305–313. http://dx.doi.org/10.1016/0003-2670(94)80250-5.
Petrakova, O., Klimentenok, G., Panov, A., Gorbachev, S., 2014. Application of modern methods for red mud processing to produce rare earth elements. 4-7 September 2014 In: Balomenos, E., Panias, D., Paspaliaris, I. (Eds.), Book of Proceedings. Presented at the ERES2014: 1st European Rare Earth Resources Conference. Heliotopos Conferences Ltd.,, Milos, Greece, pp. 221–229.
Petrascheck, W.E., 1989. The genesis of allochthonous karst-type bauxite deposits of Southern Europe. Miner. Deposita 24, 77–81. http://dx.doi.org/10.1007/BF00206306.
Pontikes, Y., 2007. Utilisation of red mud in the heavy clay industry (Αξιοποίηση της ερυθράς ιλύος στη βιομηχανία παραδοσιακών κεραμικών) (PhD thesis, in Greek). University of Patras, Department of Chemical Engineering, Patras, Greece. http://dx.doi.org/10.12681/eadd/18054.
Radusinović, S., Jelenković, R., Pačevski, A., Simić, V., Božović, D., Holclajtner-Antunović, I., Životić, D., 2017. Content and mode of occurrences of rare earth elements in the Zagrad karstic bauxite deposit (Nikšić area, Montenegro). Ore Geol. Rev. 80, 406–428. http://dx.doi.org/10.1016/j.oregeorev.2016.05.026.
Rivera, R.M., Ounoughene, G., Borra, C.R., Binnemans, K., Van Gerven, T., 2017. Neutralisation of bauxite residue by carbon dioxide prior to acidic leaching for metal recovery. Miner. Eng. 112, 92–102. http://dx.doi.org/10.1016/j.mineng.2017.07.011.
Ruan, H.D., Frost, R.L., Kloprogge, J.T., 2001. Comparison of Raman spectra in characterizing gibbsite, bayerite, diaspore and boehmite. J. Raman Spectrosc. 32, 745–750. http://dx.doi.org/10.1002/jrs.736.
Rudnick, R.L., Gao, S., 2003. 3.01 - Composition of the Continental Crust. In: Holland, H.D., Turekian, K.K. (Eds.), Treatise on Geochemistry. Pergamon, Oxford, pp. 1–64. http://dx.doi.org/10.1016/B0-08-043751-6/03016-4.
Sajó, I.E., 2008. X-ray diffraction quantitative phase analysis of Bayer process solids. In: Proceedings of The10th International Congress of ICSOBA. Presented at the 10th International Congress of ICSOBA, Bhubaneshwar, India, 28–30 November 2008, pp. 71–76.
Sajó, I.E., 2005. XDB powder diffraction phase analytical system, version 3.107; Software, Copyright Sajó, I.E. 1987–2016; Sajó, I.E.: Budapest, Hungary.
Samson, I.M., Chassé, M., 2016. Scandium. In: White, W.M. (Ed.), Encyclopedia of Geochemistry, Encyclopedia of Earth Sciences Series. Springer International Publishing, Cham, Switzerland, pp. 1–5. http://dx.doi.org/10.1007/978-3-319-39193-9_281-1.
Smith, P., 2017. Reactions of lime under high temperature Bayer digestion conditions. Hydrometallurgy, Hydrometallurgy Special Issue: AQW Conference 2015 (170), 16–23. http://dx.doi.org/10.1016/j.hydromet.2016.02.011.
Songqing, G., Zhonglin, Y., 2016. Preheaters and digesters in the Bayer digestion process. In: Essential Readings in Light Metals. Springer, Cham, pp. 356–361. http://dx.doi.org/10.1007/978-3-319-48176-0_47.
Suss, A., Kuznetsova, N.V., Kozyrev, A., Panov, A., Gorbachev, S., 2017. Specific features of scandium behavior during sodium bicarbonate digestion of red mud. In: Proceedings, Travaux 46. Presented at the 35th International ICSOBA Conference, ICSOBA, Hamburg, Germany, 2-5 October, pp. 491–504.
Suss, A.G., Rydashevsky, L.S., 1996. Behaviour of bauxite titanium minerals in Bayer process and their influence on the incrustation of heating surfaces. Methods of deposits prevention. In: Proceedings, Travaux No. 27. Presented at the 11th International Symposium of ICSOBA, Balatonfüred, Hungary, 21-24 May 1996.
Valeton, I., Biermann, M., Reche, R., Rosenberg, F., 1987. Genesis of nickel laterites and bauxites in Greece during the Jurassic and Cretaceous, and their relation to ultrabasic parent rocks. Ore Geol. Rev. 2, 359–404. http://dx.doi.org/10.1016/0169-1368(87)90011-4.
Vind, J., Alexandri, A., Vassiliadou, V., Panias, D., 2018. Distribution of selected trace elements in the Bayer Process. Submitted to Metals on 9.4.2018.
Vind, J., Paiste, P., Tkaczyk, A.H., Vassiliadou, V., Panias, D., 2017. The behaviour of scandium in the Bayer process. In: Book of Abstracts. Presented at the 2nd Conference on European Rare Earth Resources, Heliotopos Conferences Ltd., Santorini, Greece, 28-31 May 2017, pp. 190–191.
Wagh, A.S., Pinnock, W.R., 1987. Occurrence of scandium and rare earth elements in Jamaican bauxite waste. Econ. Geol. 82, 757–761. http://dx.doi.org/10.2113/gsecongeo.82.3.757.
Whittington, B.I., 1996. The chemistry of CaO and $Ca(OH)_2$ relating to the Bayer process. Hydrometallurgy 43, 13–35. http://dx.doi.org/10.1016/0304-386X(96)00009-6.
Xiao, J., 1996. Distribution characteristics of scandium in the red mud of industrial wastes. Geol. Geochem. 82–86.
Yagmurlu, B., Dittrich, C., Friedrich, B., 2017. Precipitation trends of scandium in synthetic red mud solutions with different precipitation agents. J. Sustain. Metall. 3, 90–98. http://dx.doi.org/10.1007/s40831-016-0098-9.
Zhang, N., Li, H.-X., Cheng, H.-J., Liu, X.-M., 2017. Electron probe microanalysis for revealing occurrence mode of scandium in Bayer red mud. Rare Met. 36, 295–303. http://dx.doi.org/10.1007/s12598-017-0893-x.
Zhang, N., Li, H.-X., Liu, X.-M., 2016. Recovery of scandium from bauxite residue—red mud: a review. Rare Met. 35, 887–900. http://dx.doi.org/10.1007/s12598-016-0805-5.
Zhong-Lin, Y., Song-Qing, G., 1995. Development of research on the scaling problem in Bayer process. Light Met. 155–159.